Force field for halide and alkali ions in water based on single-ion and ion-pair thermodynamic properties for a wide range of concentrations

Maria Duenas-Herrera ; Douwe Jan Bonthuis ; Philip Loche ; Roland R. Netz ; Laura Scalfi ✉
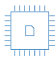
Check for updates

View Online   Export Citation

Force field for halide and alkali ions in water based on single-ion and ion-pair thermodynamic properties for a wide range of concentrations

View Online   Export Citation   CrossMark

Maria Duenas-Herrera,[1,2] (ID) Douwe Jan Bonthuis,[3] (ID) Philip Loche,[1,4] (ID) Roland R. Netz,[1] (ID) and Laura Scalfi[1,a)] (ID)

AFFILIATIONS

[1] Fachbereich Physik, Freie Universität Berlin, Arnimallee 14, 14195 Berlin, Germany
[2] Max Planck Institute for Polymer Research, Ackermannweg 10, 55128 Mainz, Germany
[3] Institute of Theoretical and Computational Physics, Graz University of Technology, Graz, Austria
[4] Laboratory of Computational Science and Modeling, IMX, Ecole Polytechnique Federale de Lausanne, 1015 Lausanne, Switzerland

[a)] Author to whom correspondence should be addressed: laura.scalfi@fu-berlin.de

ABSTRACT

A classical non-polarizable force field for the common halide (F^-, Cl^-, Br^-, and I^-) and alkali (Li^+, Na^+, K^+, and Cs^+) ions in SPC/E water is presented. This is an extension of the force field developed by Loche *et al.* for Na^+, K^+, Cl^-, and Br^- (JPCB 125, 8581–8587, 2021): in the present work, we additionally optimize Lennard-Jones parameters for Li^+, I^-, Cs^+, and F^- ions. Li^+ and F^- are particularly challenging ions to model due to their small size. The force field is optimized with respect to experimental solvation free energies and activity coefficients, which are the necessary and sufficient quantities to accurately reproduce the electrolyte thermodynamics. Good agreement with experimental reference data is achieved for a wide range of concentrations (up to 4 mol/l). We find that standard Lorentz–Berthelot combination rules are sufficient for all ions except F^-, for which modified combination rules are necessary. With the optimized parameters, we show that, although the force field is only optimized based on thermodynamic properties, structural properties are reproduced quantitatively, while ion diffusion coefficients are in qualitative agreement with experimental values.

I. INTRODUCTION

Accurately describing the behavior of electrolyte solutions at the molecular scale is important in a variety of fields, such as electrochemistry and energy storage, biology, and geoscience. Molecular simulations and statistical mechanics can predict macroscopic properties such as capacitance, conductivity, and structural and transport properties, as well as thermodynamic quantities. However, these studies heavily rely on the underlying model: when performing force field molecular dynamics, the accuracy of the results depends sensitively on the force field parameters. Several popular ionic force fields[3–5] accurately describe many electrolyte properties, such as the ionic solvation structure or density; however, they often fail to reproduce collective properties such as solubilities, viscosities, and osmotic and activity coefficients.[6–8] These collective properties

are fundamental for concentrated electrolytes relevant for biology, geoscience, or technological applications and have to be explicitly considered in force field optimization in order to be correctly reproduced.[7,9]

In this context, force fields for ions in water without explicit polarizability have been developed and improved in the last decades and have been successfully used to study a wide range of electrolyte and ionic systems, ranging from charged interfaces to polypeptides.[10–13] These force fields aim at correctly describing the thermodynamics of the solution by reproducing a single-ion property, namely, the solvation free energy, as well as a collective quantity, that can capture the behavior of ion pairs at different concentrations. Different ion-pair quantities have been used in the literature, such as the crystal lattice energy,[3] the solvation entropy,[14] or the osmotic coefficient.[15–17] These choices, however, often lead to

26 August 2024 10:15:13

TABLE I. Optimized Lennard-Jones parameters, defined in Eq. (1), and ionic charge q developed in this work and from Loche et al.[25]

	Li$^+$	Na$^+$	K$^+$	Cs$^+$	F$^{-\,a}$	Cl$^-$	Br$^-$	I$^-$
σ_{ii} (nm)	0.1285	0.231	0.283	0.3331	0.37	0.43	0.443	0.473
ϵ_{ii} (kJ/mol)	2.525	0.45	0.90	1.54	0.1	0.42	0.75	1.38
q [e]	+1	+1	+1	+1	−1	−1	−1	−1

[a]For fluoride, non-standard combination rules are needed, as defined in Eq. (2) and given in Table II.

unsatisfactory properties for certain ions so that another route was proposed based on activity coefficients.[18–25] Indeed, the activity is a fundamental thermodynamic property probing ion–ion interactions in electrolyte solutions.

Standard ionic force fields are based on the Coulomb potential for electrostatic interactions and the Lennard-Jones (LJ) potential for intermolecular interactions,

$$U_{LJ} = \sum_{i<j} 4\epsilon_{ij}\left(\frac{\sigma_{ij}^{12}}{r_{ij}^{12}} - \frac{\sigma_{ij}^{6}}{r_{ij}^{6}}\right) \qquad \text{for } r_{ij} < r_{\text{cut}}, \qquad (1)$$

where r_{ij} is the distance between atoms i and j and the sum runs over all atomic pairs closer than a cutoff value r_{cut}. The LJ parameters to be optimized are ϵ_{ij} and σ_{ij}, which quantify the strength of the interaction and its range, respectively. The LJ potential is a non-polarizable force field, i.e., it includes polarization effects implicitly but does not take into account any explicit polarizability. This choice spawns from the large flexibility of the LJ potential, which has two independent parameters for each interaction. This leads to a large parameter space, which is under-explored in the literature; for example, for a simple salt in water, excluding water self-interactions, there are 10 LJ parameters that can be tuned that describe the interactions between the water oxygen atoms, the cations, and the anions. Adding additional parameters to the model, such as explicit polarizability[26–29] or fractional ionic charges,[30] can actually be avoided by exploring the full parameter space of the LJ potential. We can reparameterize this parameter space by using like-species parameters $\sigma_i \equiv \sigma_{ii}$ and $\epsilon_i \equiv \epsilon_{ii}$ and defining combination rules, for example,

$$\sigma_{ij} = \lambda_\sigma^{ij}\frac{\sigma_i + \sigma_j}{2}, \qquad \epsilon_{ij} = \lambda_\epsilon^{ij}\sqrt{\epsilon_i \epsilon_j}, \qquad (2)$$

where λ_σ^{ij} and λ_ϵ^{ij} are the two parameters that allow to obtain mixed-species parameters. In practice, the parameter space is often reduced for easy transferability by using the standard Lorentz–Berthelot combination rules, i.e., by setting $\lambda_\sigma^{ij} = \lambda_\epsilon^{ij} = 1$. For a few ions, however, it was found that the standard combination rules for intermolecular parameters do not allow for the reproduction of both the solvation free energy and the activity coefficients. This problem is solved by additionally optimizing the λ_σ^{ij} and λ_ϵ^{ij} parameters.[21–24,31] In the following, we use the standard Lorentz–Berthelot combination rules, except where stated otherwise.

A drawback of previous studies is that the optimization procedure requires a reference ion to be fixed, in most cases chloride.[14,17,19–24] Recently, a non-polarizable force field was developed using a global optimization procedure that does not require

TABLE II. Optimized Lennard-Jones parameter λ_σ^{ij}, defined in Eq. (2), developed in this work for ion pairs including fluoride. We keep the parameter $\lambda_\epsilon^{ij} = 1$. For all other ion pairs we have $\lambda_\sigma^{ij} = \lambda_\epsilon^{ij} = 1$.

	NaF	KF	CsF
λ_σ^{ij}	1.0	1.5	1.4

any prior assumptions on the parameters of any ion.[25] This force field was developed for four ions: Na$^+$, K$^+$, Cl$^-$, and Br$^-$. Following these previous efforts, we extend here the non-polarizable force field introduced by Loche et al.[25] by additionally optimizing parameters for the common alkali and halide ions, i.e., Li$^+$, Cs$^+$, F$^-$, and I$^-$. This extension is, therefore, also reference-free since it is built on the previous globally optimized force field. The optimized parameters are presented in Tables I and II.

II. FORCE FIELD OPTIMIZATION

The scope of this work is to optimize Lennard-Jones parameters of ions in SPC/E water[32] by reproducing their experimental solvation free energies and activity coefficients, starting from the known ion parameters developed for Na$^+$, K$^+$, Cl$^-$, and Br$^-$ in Ref. 25. In a nutshell, for each additional cation (respectively anion), we consider the ion pairs formed with the two known anions (respectively cation) and extract a free energy isoline in the $\sigma - \epsilon$ parameter plane corresponding to the experimental solvation free energy of the salt [see Figs. 1(a) and 1(b)]. For a set of LJ parameters along the isoline, we then compute the activity derivatives in a wide concentration range from 0.5 to 4 mol/l. The optimal parameters are determined by minimizing the root mean square deviation from the experimental activity reference data.

A. Solvation free energy

The solvation free energy ΔF is a single-ion property, i.e., although experimental data are only available for ion pairs, the solvation free energy of a salt ij can be decomposed in the dilute limit into single-ion components as $\Delta F^{ij} = \Delta F^i + \Delta F^j$.

In order to span the full parameter space, we compute the single-ion solvation free energy by thermodynamic integration for a wide range of Lennard-Jones parameters $\{\sigma, \epsilon\}$, both for a cation ($q = +1$) and an anion ($q = -1$). Methodological details are given in Sec. S1 of the supplementary material, along with the full solvation free energy maps (see Fig. S1 in the supplementary material). For
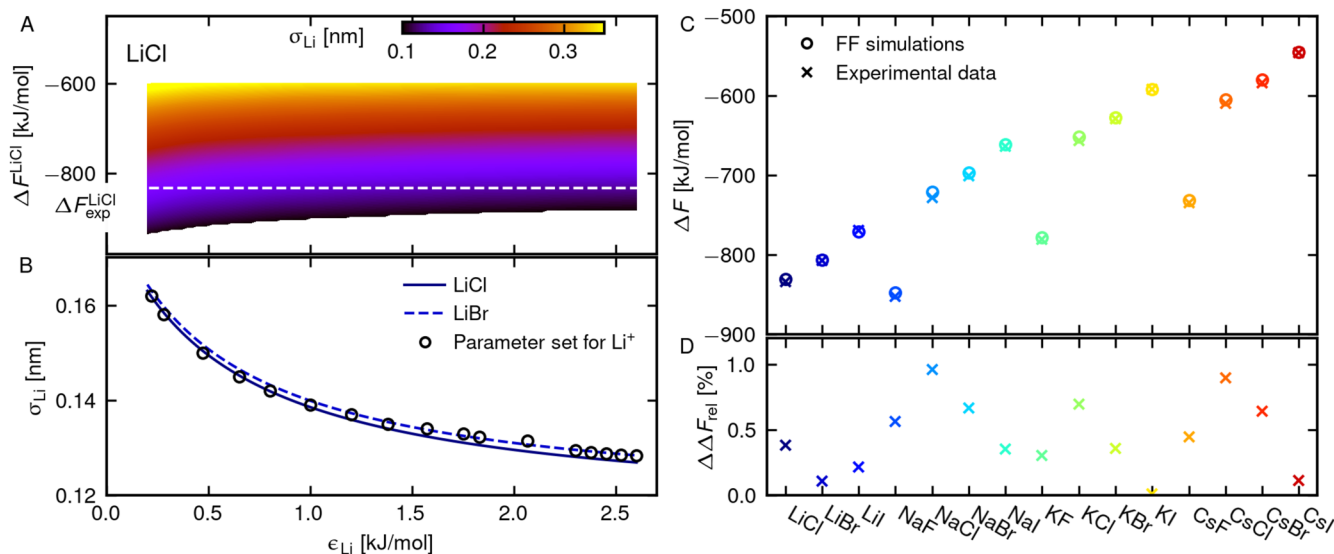
FIG. 1. (a) Colormap of the σ_{Li} parameter yielding a given solvation free energy ΔF^{LiCl} for a given value of ϵ_{Li} for LiCl in the infinite dilution limit, using the previously optimized σ_{Cl} and ϵ_{Cl}. This map was obtained from the cubic spline interpolations from Fig. S1 in the supplementary material. The horizontal white dashed line indicates the experimental solvation free energy for the LiCl salt. (b) Solvation free energy isolines giving σ_{Li} as a function of ϵ_{Li} for LiCl (solid line) and LiBr (dashed line). The lines are fits to the data (not shown) of the form $\sigma = A/(\epsilon + B) + C$ (see Sec. S1 of the supplementary material for the fitting parameters). The parameter set for Li$^+$ selected for the activity simulations is shown using empty black circles. (c) Interpolated solvation free energy of the considered salts obtained from thermodynamic integration using our optimized force field (circles) compared with experimental data from Tissandier *et al.*[1] and Marcus[2] (crosses). (d) Relative error for the solvation free energy $\Delta\Delta F_{rel} = |\Delta F - \Delta F_{exp}|/|\Delta F_{exp}|$ for each salt.

better handling, the single-ion solvation free energy values are interpolated using cubic splines. Note that the free energy map obtained in Ref. 25 is extended to cover a wider range of parameters.

For clarity, we illustrate the optimization procedure using the example of Li$^+$: we consider the salts LiCl and LiBr, for which we know the experimental solvation free energy[1,2] ΔF_{exp}^{LiCl} [horizontal dashed line in Fig. 1(a)] and ΔF_{exp}^{LiBr}. For these salts, we take the previously optimized anion parameters[25] and determine the anion solvation free energies ΔF^{Cl} and ΔF^{Br} using the solvation free energy map for anions [shown in Fig. S1(B)]. Using the free energy map for cations [shown in Fig. S1(A) projected onto the $\{\sigma, \epsilon\}$ plane and in Fig. 1(a) projected onto the $\{\epsilon, \Delta F\}$ plane], we can obtain single-ion solvation free energies for any set of Lennard-Jones parameters for Li$^+$. This allows us to extract a solvation free energy isoline for each salt, i.e., a line in the $\{\sigma_{Li}, \epsilon_{Li}\}$ parameter space for which the computed solvation free energy is equal to the experimental values for the considered salt. The isolines, plotted in Fig. 1(b) and obtained independently for the LiCl and LiBr salts, are identical up to a small deviation, so we draw parameters from the average between the two isolines. This is also true for I$^-$ and F$^-$, for which we find consistent isolines for different cations (see Fig. S2 in the supplementary material). For Cs$^+$, we consider only two LJ parameter combinations, taken from Fyta and Netz,[21] named Cs(6) and Cs(9). These parameters reproduce the solvation free energy of Cs$^+$ and were optimized against the activity derivative at 0.3 and 1 mol/l. Given the excellent agreement for the activity coefficients obtained for Cs(9) up to 4 mol/l [see Figs. 2(n)–2(o)], we do not need to further optimize the Cs$^+$ parameters.

To *a posteriori* validate our optimized force field, given in Tables I–II, we plot in Fig. 1(c) the solvation free energy for all possible ion combinations (except LiF due to its very low solubility), which show excellent agreement with experimental data,[1,2] as shown by the relative errors lower than 1% in Fig. 1(d).

B. Activity coefficients

For each LJ parameter combination extracted from isolines, such as given in Fig. 1(b), we run extensive molecular dynamics (MD) simulations of the corresponding salts (LiCl and LiBr for the example of Li$^+$) for concentrations c of 0.5, 1, 2, 3, and 4 mol/l, except for NaF, for which we studied concentrations only up to 0.5 mol/l due to its low solubility limit. In the following, however, we present results as a function of molality b (in mol/kg) instead, because most experimental data are given on this scale.

Instead of directly computing activity coefficients, we extract activity derivatives a_{cc} as

$$a_{cc} = \frac{\partial \ln a_c}{\partial \ln c} = 1 + \frac{\partial \ln \gamma_c}{\partial \ln c} = \frac{G_{+-}^{\infty} - G_{++}^{\infty}}{2(G_{+-}^{\infty} - G_{+s}^{\infty})}, \quad (3)$$

where $a_c = \gamma_c c$ is the molar activity, γ_c is the molar activity coefficient, and c is the molarity (or concentration, in mol/l). Indeed, activity derivatives a_{cc} can directly be computed from MD simulations according to the last equality in Eq. (3), using the Kirkwood–Buff (KB) formalism[36] developed for electrolytes by Kusalik and Patey.[37] $G_{\alpha\beta}^{\infty}$, where $\alpha, \beta \in \{+, -, s\}$ denote the cation, the anion, and the solvent, respectively, are KB integrals defined for
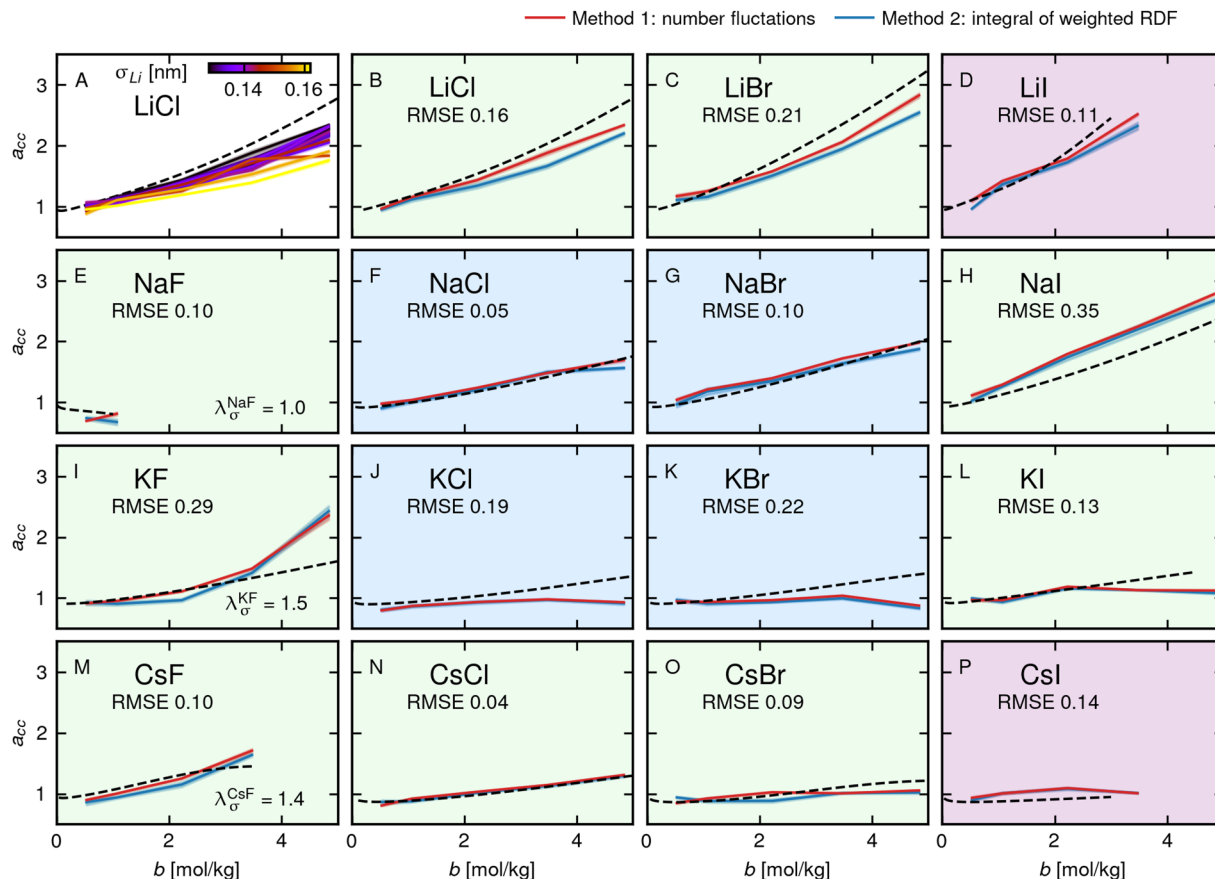
FIG. 2. (a) Activity derivatives a_{cc} for LiCl as a function of molality b for the set of LJ parameters extracted from the isoline in Fig. 1(b). (b)–(p) Activity derivatives a_{cc} as a function of molality b for the different investigated salts using the optimized LJ parameters reported in Tables I and II, evaluated using the number fluctuations method[33] (red solid lines) and the integration of weighted radial distribution functions[34] (blue solid lines). Error bars are computed from the standard error over 5 blocks. The experimental reference data (dashed black lines) are taken from Hamer and Wu.[35] The root mean squared error [Eq. (6)] averaged over the concentrations for which there are experimental data available is indicated. The panels colored in blue correspond to salts optimized by Loche *et al.*; those colored in green are the ion pairs we used to optimize our force field extension; and the two panels colored in purple are results for ion pairs that are not included in our optimization procedure.

an infinite open system as

$$G_{\alpha\beta}^{\infty} = V \left(\frac{\langle N_\alpha N_\beta \rangle - \langle N_\alpha \rangle \langle N_\beta \rangle}{\langle N_\alpha \rangle \langle N_\beta \rangle} - \frac{\delta_{\alpha\beta}}{\langle N_\alpha \rangle} \right) \quad (4)$$

$$= \frac{1}{V} \int_V \int_V d\mathbf{r}_1 d\mathbf{r}_2 (g_{\alpha\beta}(\mathbf{r}_2 - \mathbf{r}_1) - 1), \quad (5)$$

where V is the volume, N_α is the number of α particles in V, $\delta_{\alpha\beta}$ is the Kronecker delta, $\langle \cdots \rangle$ is a grand-canonical (μVT) ensemble average, and $g_{\alpha\beta}$ is the radial distribution function between species α and β. In practice, however, approximations need to be made in order to extract KB integrals from canonical NVT finite-size simulations. In this work, we extract activity coefficients using a method introduced by Cortes–Huerto *et al.*[33,38] based on Eq. (4) and number fluctuations in subvolumes of the simulation box. This method corrects for effects due to the thermodynamic ensemble and due to the finite size of the simulation cell. For comparison with earlier studies, we also calculate activity derivatives using a method based on Eq. (5) and the

integral of weighted radial distribution functions that corrects for finite-size effects and the slow convergence of KB integrals.[34] Both methods give equivalent results, as shown in Fig. 2. Technical details are given in Sec. S2 of the supplementary material.

The molar activity derivatives as a function of molality b (in mol/kg) for the selected LJ parameters are shown for LiCl in Fig. 2(a) and for all other salts in Sec. S3 of the supplementary material. To quantify the performance of each LJ parameter combination, we linearly interpolate $a_{cc}(b)$ and use the root mean square error,

$$\text{RMSE} = \sqrt{\langle (a_{cc}(b) - a_{cc}^{\exp}(b))^2 \rangle_b}, \quad (6)$$

where $\langle \ldots \rangle_b$ denotes the average over the concentration range and $a_{cc}^{\exp}$ the reference experimental data from Hamer and Wu[35] (shown as dashed black lines in Figs. 2 and 3). The optimal parameter combination is determined by minimizing the average root mean squared error (RMSE) between the two investigated salts for each ion, i.e.,
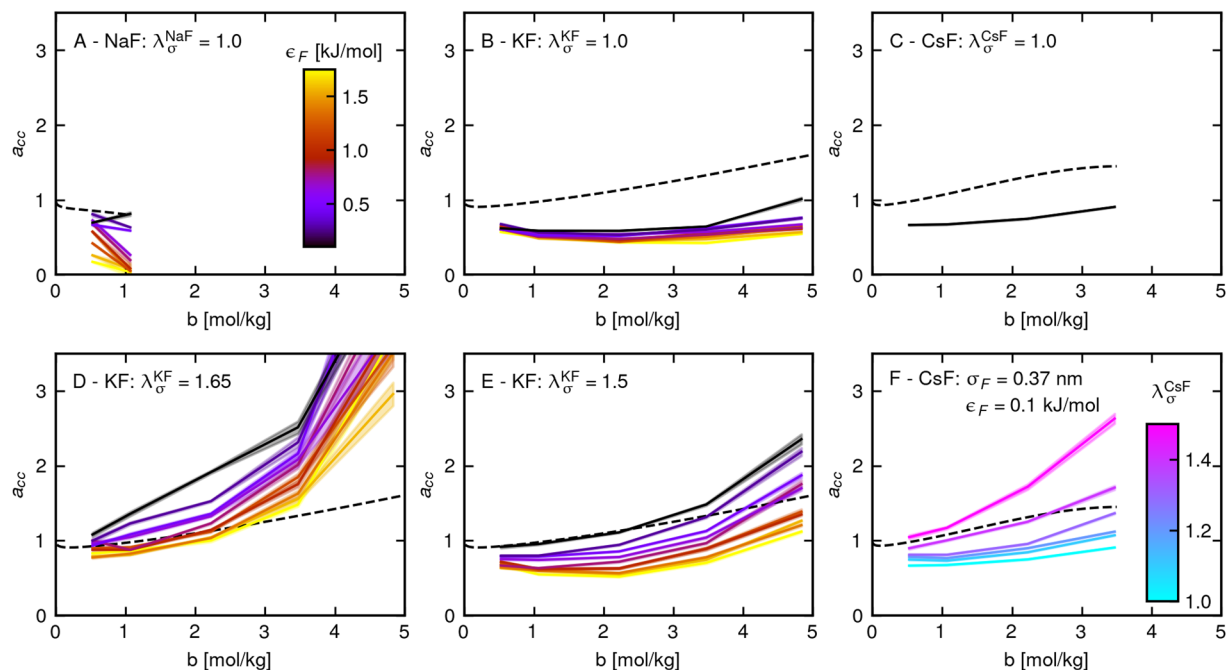
FIG. 3. Activity derivatives for NaF (a), KF (b), (d), and (e) and CsF (c) and (f) as a function of molality b, using the standard combination rules [see Eq. (2)], i.e., with $\lambda_\sigma^{ij} = 1.0$ (a)–(c), $\lambda_\sigma^{ij} = 1.65$ (d) as suggested in Fyta and Netz,[21] $\lambda_\sigma^{ij} = 1.5$ (e), and for a range of λ_σ^{ij} values (f). In panels a, b, d, and e, the activity derivatives are shown for the set of LJ parameters obtained from the solvation free energy isolines for F$^-$, while in panels c and f, only simulation results for the optimal LJ parameters $\sigma_F = 0.37$ nm and $\epsilon_F = 0.1$ kJ/mol are shown. In all panels, experimental reference data from Hamer and Wu[35] are shown with dashed lines.

[RMSE(LiCl) + RMSE(LiBr)] in the case of Li$^+$. Using this procedure, we find the optimal parameter combinations for Li$^+$, Cs$^+$, and I$^-$, reported in Table I. The activity derivative a_{cc} as a function of molality b for the optimal parameters is shown in Figs. 2(b)–2(p). The number fluctuation method[33] (red solid lines) and the radial distribution function weighted integration (blue solid lines) show good agreement in all cases, validating our evaluation of the activity coefficients. For the optimized ion pairs (LiCl, LiBr, NaI, KI, CsCl, and CsBr), we observe good agreement with the experimental values (black dashed lines), although there are still small differences between the prediction of our force field and the reference data for Li$^+$ and I$^-$. We cannot improve the agreement by going to even lower σ_i because the solvation free energy isolines reach a plateau for small σ_i and large ϵ_i [see Fig. 1(a)]. A better agreement could be found by tuning the combination rules, but this is not done in the present work. Note that the optimized σ_i values shown in Table I increase with the atomic number, as expected, together with the ϵ_i values. Li$^+$ is an outlier, with an exceptionally large ϵ_{Li}, which regulates the number of contact ion pairs in the system with respect to hydration by water molecules (see the radial distribution functions in Fig. S19 in the supplementary material).

However, for KF, no parameter combination yields values for the activity derivative close to the experimental ones for $\lambda_\sigma^{KF} = 1$, as shown in Fig. 3(b), with an RMSE of at least 0.62. Using the parameters giving the closest fit for CsF, shown in Fig. 3(c), also indicates that the standard Lorentz–Berthelot combination rules fail at fitting the activity derivative of CsF. This issue was pointed out previously by Fyta and Netz[21] and is related to the unique hydration of the

fluoride ion, shown also by the very favorable solvation free energy of its salts [see Fig. 1(c)]. To resolve this, Fyta and Netz[21] introduced modified combination rules for the cation–anion LJ parameters given in Eq. (2). Note that modifying the cation–anion parameters does not influence the solvation free energy since the cation–water and anion–water interaction parameters are kept fixed. Fyta and Netz[21] showed that λ_ϵ^{ij} does not have a significant influence on the salt activity, while they successfully tuned λ_σ^{ij} to optimize their force field for a concentration of 1 mol/l. This effectively increases the equilibrium cation–anion distance. Accordingly, we only tune in this work the value of λ_σ^{ij} and keep $\lambda_\epsilon^{ij} = 1.0$, but note that both could in principle be optimized for a better fit. Figures 3(a)–3(c) further indicate that no single λ_σ^{ij} value can describe all fluoride salts. This can further be seen in Fig. S17 in the supplementary material, where we show the activity for an arbitrary LJ parameter set as a function of λ_σ^{ij} for both KF and CsF.

We thus performed a screening of the LJ parameters for KF using the value of $\lambda_\sigma^{ij} = 1.65$ optimized in Ref. 21 and for $\lambda_\sigma^{ij} = 1.5$, shown in Figs. 3(d) and 3(e). For $\lambda_\sigma^{ij} = 1.65$, the activity derivative for high concentrations (> 3 mol/l) is highly overestimated for all parameters. This is even more drastic in the case of CsF (see Fig. S16 in the supplementary material). Using $\lambda_\sigma^{KF} = 1.5$ shows an improvement in the agreement at high concentrations with the experimental data. Applying Eq. (6) to the screening for KF for $\lambda_\sigma^{KF} = 1.5$ and the screening for NaF for $\lambda_\sigma^{NaF} = 1.0$, we find the optimal parameters for F$^-$ to be $\sigma_F = 0.37$ nm and $\epsilon_F = 0.1$ kJ/mol. To obtain results for CsF with these optimal parameters, we further

do a full screening of the λ_σ^{CsF} parameter as a function of molality b, shown in Fig. 3(f), and using Eq. (6), we determine the optimal combination rule to be given by $\lambda_\sigma^{CsF} = 1.4$.

The activity derivatives for the optimal LJ parameters (σ_F, ϵ_F, and λ_σ^{ij}) are plotted in Figs. 2(e), 2(i), and 2(m). These show good agreement with experimental data, except for a deviation above 3 mol/l for KF, meaning that the force field for KF is only expected to work well at concentrations below 3 mol/l.

III. RESULTS AND DISCUSSION

A. Transferability

Transferability is an important quality for a force field when it is used in combination with species that were not considered during the force field optimization. In the previous work by Loche *et al.*,[25]

the authors showed good transferability of the ionic parameters to other water models, i.e., TIP3P, TIP4P, and TIP4P/ϵ, except for a worse performance in the case of TIP4P water with NaBr. These results suggest that our parameters should also be transferable to other water models.

Moreover, we computed activity derivatives for ion pairs that were not considered in the optimization, namely, LiI and CsI (LiF was not studied because no experimental data were found as a reference). The results are shown in Figs. 2(d) and 2(p) and show excellent agreement with the experimental data, demonstrating a good transferability of the Li$^+$, I$^-$, and Cs$^+$ parameters using standard Lorentz–Berthelot combination rules. For F$^-$, however, we found that the combination rule for the cation–anion interaction is ion-pair dependent and should be re-optimized for each new ion pair.
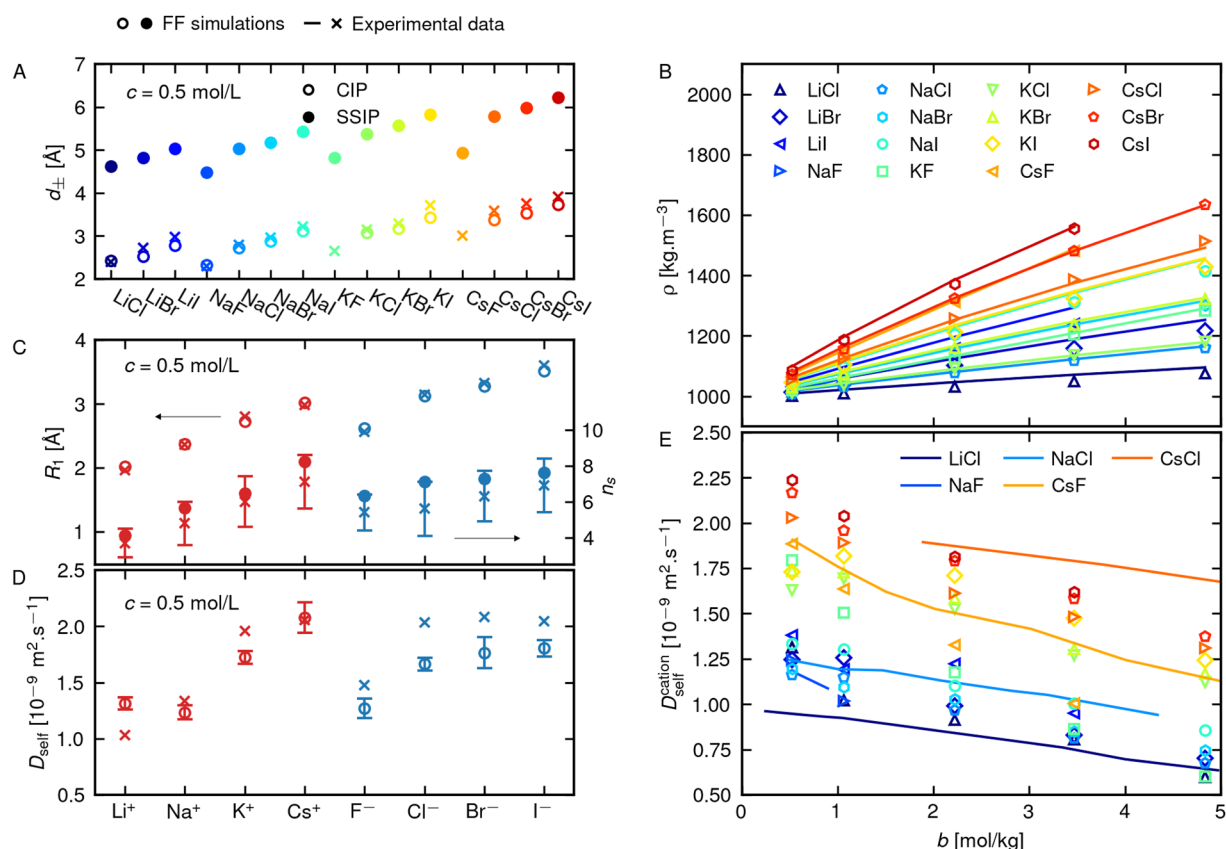

FIG. 4. (a) Contact ion pair (CIP: empty circles) and solvent separated ion pair (SSIP: full circles) distances, taken from the first and second maxima of the cation–anion radial distribution function, at a concentration of 0.5 mol/l, compared with experimental bond lengths (crosses) from crystallographic data of the corresponding solid salts from the Materials Project.[39] Note that in the case of KF and CsF, no CIP is observed in our simulations. (b) Computed densities of the different salts as a function of molality b (symbols) compared to experimental fits (solid lines: one line per salt) from Harned *et al.*[40] of the form $c = d_0 b - Ab^2 + Bb^3$ and Pedersen *et al.*[41] (c) Effective ionic radii (empty circles, left axis), taken as the position of the first maximum in the simulated ion–water radial distribution function, averaged over the different salts containing the specified ion at a concentration of 0.5 mol/l, compared with experimental data (crosses).[42] Computed coordination numbers (filled circles, right axis), taken as the integral over the ion–water radial distribution function up to the first minimum, averaged over the different salts containing the specified ion at a concentration of 0.5 mol/l, compared with experimental data (crosses with error bars).[42] (d) Computed self-diffusion coefficient of ions (empty circles), averaged over the different salts containing the specified ion, at a concentration of 0.5 mol/l, compared to experimental data (crosses) from Marcus.[2] (e) Computed self-diffusion coefficient of the cations (symbols) for the different salts as a function of molality b, compared to experimental data taken from Braun and Weingaertner[43] (data are available only for a few salts, indicated in the legend).

B. Solvation structure

Many force fields are optimized based on structural properties such as the salt solution density or the effective ion size. We first investigate the ion pairing behavior in the studied electrolytes based on the cation–anion radial distribution functions (RDF: shown as a function of concentration in Sec. S4 of the supplementary material). The RDFs show a first peak between 2 and 4 Å that corresponds to a contact ion pair (CIP), followed by a second broader peak corresponding to a solvent-separated ion pair (SSIP). The position of these peaks at the lowest concentration of 0.5 mol/l is shown in Fig. 4(a) for all ion pairs (open circles for CIP and filled circles for SSIP). For KF and CsF, however, we do not observe the formation of CIP in solution due to the large σ_{KF} and σ_{CsF} obtained using the modified combination rules. Note that these large σ values mostly have an impact on the cation–anion RDF, as shown in Fig. S20 of the supplementary material, which is necessary to reproduce the experimental activity coefficients. Experimentally, determining the relative weights of CIP, SSIP, and fully solvated ions in electrolytes and their dependence on concentration is very challenging, resulting in debated and conflicting results.[44–51] It is thus unclear how the simulated RDFs relate to the experiments. Nevertheless, we observe that our SSIP distances for KF and CsF are in line with the expected trends. For all other ion pairs, the CIP distances show good agreement with experimental ionic distances computed from the salt crystal lattice[39] (crosses).

To evaluate the ability of our force field to reproduce the solvation structure using available experimental data, we further extract an effective ion size from the position of the first maximum in the ion–water radial distribution function $g_{\pm s}$ at the lowest concentration of 0.5 mol/l (the radial distribution functions as a function of concentration are given in Sec. S4 of the supplementary material). Results are plotted in Fig. 4(c) (empty circles) and show quantitative agreement with experimental data (crosses) from Marcus.[42] In addition, we show water coordination numbers (filled circles), computed as the integral of $g_{\pm s}$ over the first solvation layer (i.e., up to its first minimum), which also show good agreement with recent experimental values (crosses).[42]

To assess the global structure, we further compute the density from our MD simulations as a function of concentration (symbols) and compare it with experimental data (solid lines) in Fig. 4(b). We find very good agreement over the full range of concentrations, which confirms that our force field correctly reproduces the structural properties of electrolyte solutions.

C. Dynamics

The force field optimized in this work is designed to correctly reproduce the thermodynamic properties of single ions and their solutions, up to a concentration of ~4 mol/l. The good agreement of the microscopic structure shown above is encouraging regarding the ability of the force field to also capture the dynamics of a system. To check this, we investigate the ionic self-diffusion coefficient D_{self} in the most dilute systems $c = 0.5$ mol/l, obtained as 1/6 of the long-time slope of the mean squared displacement of the ions MSD(τ) $= \langle [\mathbf{r}(t + \tau) - \mathbf{r}(t)]^2 \rangle$, where the average is over the initial times t and all ions in the box. We additionally used the Yeh–Hummer correction[52] to correct for the finite size of our simulation box. In Fig. 4(d), we plot the average over all investigated salts containing

a given ion; the error bars denote the standard deviation among the different salt solutions. The results show deviations from the experimental values smaller than 0.5×10^{-9} m^2 s^{-1}, which is a good performance given the deviations of the viscosity of the simulated SPC/E water from experimental values. We also observe the same qualitative trends, i.e., the self-diffusion coefficient roughly follows the evolution of the ion size.

In Fig. 4(e), we present the self-diffusion coefficient of cations as a function of molality for different salts. We observe some deviations from the experimental values but are able to reproduce correctly the decrease in the self-diffusion coefficient with concentration. Therefore, although the dynamical properties of the electrolytes are not considered in the optimization, we find satisfactory agreement and reproduce the experimental trends of the ionic diffusion coefficient with respect to ion type and concentration.

IV. CONCLUSION

In this work, we have extended the results of Loche et al.[25] by parameterizing force field parameters for lithium, iodide, cesium, and fluoride ions in water, which reproduce the solvation free energy of the single ions and the activity coefficients for a wide range of concentrations (up to 4 mol/l). Following previous studies,[21] we find that standard Lorentz–Berthelot combination rules are sufficient to describe lithium, iodide, and cesium salts, while fluoride is an exception for which a fine-tuning of the ion–ion combination rules is necessary. We further show that structural properties, such as contact ion distance, ion size, and salt solution densities, are quantitatively reproduced and that dynamical properties are in qualitative agreement with experimental values. This force field will allow thermodynamically consistent simulations of electrolytes up to high concentrations, which is essential for biological or energy applications.

V. METHODS

In this work, we simulate two kinds of systems: one at infinite dilution with a single solvated ion, and one at finite concentration. At infinite dilution, we place a single ion and 509 SPC/E water molecules[32] in a cubic box of length $L = 2.5$ nm. At finite concentration, we generate cubic simulation boxes containing SPC/E water[32] and a number of ion pairs corresponding to the desired concentration (ranging from 0.5 to 4 mol/l), with box size $L = 6.5$ nm. All molecular dynamics simulations are performed using the GROMACS software.[53] The simulation boxes are periodically replicated in all directions, and long-range electrostatics are handled using the smooth particle mesh Ewald (SPME) technique.[54] The Lennard-Jones cutoff is set to 0.9 nm, and the Lennard-Jones potential is shifted at the cutoff. All systems are first energy-minimized using the steepest descent algorithm and then equilibrated in the NPT ensemble with $P = 1$ bar and $T = 300$ K for 200 ps (the final box length L is only weakly modified), followed by a production run in the NVT ensemble of at least 1 ns for the infinite dilution systems and of 50 ns for the finite concentrations. The equations of motion are solved using the velocity Verlet algorithm using a timestep of 2 fs. For the pressure coupling, we use a Berendsen barostat[55] with a time constant of 1 ps. We use a velocity rescaling thermostat[56] with a time constant of 0.5 ps to maintain the temperature at 300 K, and we

26 August 2024 10:15:13

constrain the geometry of water molecules using the SETTLE algorithm. Details on the thermodynamic integration and methods to extract activity coefficients are given in the supplementary material.

SUPPLEMENTAL MATERIAL

The supplementary material contains details on the solvation free energy and activity coefficient calculations, as well as detailed screenings of Lennard-Jones parameters.

ACKNOWLEDGMENTS

AUTHOR DECLARATIONS

Conflict of Interest

The authors have no conflicts to disclose.

Author Contributions

Maria Duenas-Herrera: Conceptualization (equal); Investigation (equal); Methodology (equal); Visualization (equal); Writing – review & editing (equal). **Douwe Jan Bonthuis**: Conceptualization (supporting); Investigation (supporting); Methodology (supporting); Supervision (equal); Writing – review & editing (equal). **Philip Loche**: Conceptualization (equal); Investigation (equal); Methodology (equal); Supervision (supporting); Visualization (equal); Writing – review & editing (equal). **Roland R. Netz**: Conceptualization (equal); Funding acquisition (lead); Investigation (equal); Methodology (equal); Supervision (lead); Writing – review & editing (equal). **Laura Scalfi**: Conceptualization (equal); Investigation (equal); Methodology (equal); Supervision (lead); Visualization (lead); Writing – original draft (lead); Writing – review & editing (lead).

DATA AVAILABILITY

The data that support the findings are available upon reasonable request to the corresponding author. A repository containing the force field files for GROMACS as well as the solvation free energy data from Fig. S1 of the supplementary material is provided at https://gitlabph.physik.fu-berlin.de/ploche/simple-ion-force-field.

REFERENCES

[1] M. D. Tissandier, K. A. Cowen, W. Y. Feng, E. Gundlach, M. H. Cohen, A. D. Earhart, J. V. Coe, and T. R. Tuttle, "The proton's absolute aqueous enthalpy and gibbs free energy of solvation from cluster-ion solvation data," J. Phys. Chem. A **102**, 7787–7794 (1998).

[2] Y. Marcus, *Ion Properties* (Taylor & Francis, 1997).

[3] I. S. Joung and T. E. I. Cheatham, "Determination of alkali and halide monovalent ion parameters for use in explicitly solvated biomolecular simulations," J. Phys. Chem. B **112**, 9020–9041 (2008).

[4] D. E. Smith and L. X. Dang, "Computer simulations of NaCl association in polarizable water," J. Chem. Phys. **100**, 3757–3766 (1994).

[5] S. Koneshan, J. C. Rasaiah, R. M. Lynden-Bell, and S. H. Lee, "Solvent structure, dynamics, and ion mobility in aqueous solutions at 25 °C," J. Phys. Chem. B **102**, 4193–4204 (1998).

[6] I. S. Joung and T. E. I. Cheatham, "Molecular dynamics simulations of the dynamic and energetic properties of alkali and halide ions using water-model-specific ion parameters," J. Phys. Chem. B **113**, 13279–13290 (2009).

[7] A. Z. Panagiotopoulos, "Simulations of activities, solubilities, transport properties, and nucleation rates for aqueous electrolyte solutions," J. Chem. Phys. **153**, 010903 (2020).

[8] S. Blazquez, J. L. F. Abascal, J. Lagerweij, P. Habibi, P. Dey, T. J. H. Vlugt, O. A. Moultos, and C. Vega, "Computation of electrical conductivities of aqueous electrolyte solutions: Two surfaces, one property," J. Chem. Theory Comput. **19**, 5380–5393 (2023).

[9] K. Fan, Y. Zhang, Y. Qiu, and H. Zhang, "Impacts of targeting different hydration free energy references on the development of ion potentials," Phys. Chem. Chem. Phys. **24**, 16244–16262 (2022).

[10] N. J. Sinha, K. C. Cunha, R. Murphy, C. J. Hawker, J.-E. Shea, and M. E. Helgeson, "Competition between β-sheet and coacervate domains yields diverse morphologies in mixtures of oppositely charged homochiral polypeptides," Biomacromolecules **24**, 3580–3588 (2023).

[11] S. Gravelle, S. Haber-Pohlmeier, C. Mattea, S. Stapf, C. Holm, and A. Schlaich, "NMR investigation of water in salt crusts: Insights from experiments and molecular simulations," Langmuir **39**, 7548–7556 (2023).

[12] J. Hunger, J. Schaefer, P. Ober, T. Seki, Y. Wang, L. Prädel, Y. Nagata, M. Bonn, D. J. Bonthuis, and E. H. G. Backus, "Nature of cations critically affects water at the negatively charged silica interface," J. Am. Chem. Soc. **144**, 19726–19738 (2022).

[13] P. Loche, D. J. Bonthuis, and R. R. Netz, "Molecular dynamics simulations of the evaporation of hydrated ions from aqueous solution," Commun. Chem. **5**, 55–58 (2022).

[14] D. Horinek, S. I. Mamatkulov, and R. R. Netz, "Rational design of ion force fields based on thermodynamic solvation properties," J. Chem. Phys. **130**, 124507 (2009).

[15] B. Hess and N. F. A. van der Vegt, "Cation specific binding with protein surface charges," Proc. Natl. Acad. Sci. U. S. A. **106**, 13296–13300 (2009).

[16] I. Kalcher and J. Dzubiella, "Structure-thermodynamics relation of electrolyte solutions," J. Chem. Phys. **130**, 134507 (2009).

[17] M. Fyta, I. Kalcher, J. Dzubiella, L. Vrbka, and R. R. Netz, "Ionic force field optimization based on single-ion and ion-pair solvation properties," J. Chem. Phys. **132**, 024911 (2010).

[18] S. Weerasinghe and P. E. Smith, "A Kirkwood–Buff derived force field for sodium chloride in water," J. Chem. Phys. **119**, 11342–11349 (2003).

[19] B. Klasczyk and V. Knecht, "Kirkwood–Buff derived force field for alkali chlorides in simple point charge water," J. Chem. Phys. **132**, 024109 (2010).

[20] M. B. Gee, N. R. Cox, Y. Jiao, N. Bentenitis, S. Weerasinghe, and P. E. Smith, "A Kirkwood–Buff derived force field for aqueous alkali halides," J. Chem. Theory Comput. **7**, 1369–1380 (2011).

[21] M. Fyta and R. R. Netz, "Ionic force field optimization based on single-ion and ion-pair solvation properties: Going beyond standard mixing rules," J. Chem. Phys. **136**, 124103 (2012).

[22] S. Mamatkulov, M. Fyta, and R. R. Netz, "Force fields for divalent cations based on single-ion and ion-pair properties," J. Chem. Phys. **138**, 024505 (2013).

[23] D. J. Bonthuis, S. I. Mamatkulov, and R. R. Netz, "Optimization of classical nonpolarizable force fields for OH⁻ and H₃O⁺," J. Chem. Phys. **144**, 104503 (2016).

[24] S. Mamatkulov and N. Schwierz, "Force fields for monovalent and divalent metal cations in TIP3P water based on thermodynamic and kinetic properties," J. Chem. Phys. **148**, 074504 (2018).

26 August 2024 10:15:13

[25] P. Loche, P. Steinbrunner, S. Friedowitz, R. R. Netz, and D. J. Bonthuis, "Transferable ion force fields in water from a simultaneous optimization of ion solvation and ion–ion interaction," J. Phys. Chem. B **125**, 8581–8587 (2021).

[26] T. A. Halgren and W. Damm, "Polarizable force fields," Curr. Opin. Struct. Biol. **11**, 236–242 (2001).

[27] J. W. Ponder, C. Wu, P. Ren, V. S. Pande, J. D. Chodera, M. J. Schnieders, I. Haque, D. L. Mobley, D. S. Lambrecht, R. A. J. DiStasio, M. Head-Gordon, G. N. I. Clark, M. E. Johnson, and T. Head-Gordon, "Current status of the AMOEBA polarizable force field," J. Phys. Chem. B **114**, 2549–2564 (2010).

[28] T.-M. Chang and L. X. Dang, "Recent advances in molecular simulations of ion solvation at liquid interfaces," Chem. Rev. **106**, 1305–1322 (2006).

[29] H. Yu, T. W. Whitfield, E. Harder, G. Lamoureux, I. Vorobyov, V. M. Anisimov, A. D. J. MacKerell, and B. Roux, "Simulating monovalent and divalent ions in aqueous solution using a drude polarizable force field," J. Chem. Theory Comput. **6**, 774–786 (2010).

[30] I. M. Zeron, J. L. F. Abascal, and C. Vega, "A force field of Li$^+$, Na$^+$, K$^+$, Mg^{2+}, Ca^{2+}, Cl$^-$, and SO$_4^{2-}$ in aqueous solution based on the TIP4P/2005 water model and scaled charges for the ions," J. Chem. Phys. **151**, 134504 (2019).

[31] X. Zhu, P. E. M. Lopes, and A. D. MacKerell, Jr., "Recent developments and applications of the CHARMM force fields," WIREs Comput. Mol. Sci. **2**, 167–185 (2012).

[32] H. J. C. Berendsen, J. R. Grigera, and T. P. Straatsma, "The missing term in effective pair potentials," J. Phys. Chem. **91**, 6269–6271 (1987).

[33] R. Cortes-Huerto, K. Kremer, and R. Potestio, "Communication: Kirkwood–Buff integrals in the thermodynamic limit from small-sized molecular dynamics simulations," J. Chem. Phys. **145**, 141103 (2016).

[34] P. Krüger, S. K. Schnell, D. Bedeaux, S. Kjelstrup, T. J. H. Vlugt, and J.-M. Simon, "Kirkwood–Buff integrals for finite volumes," J. Phys. Chem. Lett. **4**, 235–238 (2013).

[35] W. J. Hamer and Y. Wu, "Osmotic coefficients and mean activity coefficients of uni-univalent electrolytes in water at 25 °C," J. Phys. Chem. Ref. Data **1**, 1047–1100 (1972).

[36] J. G. Kirkwood and F. P. Buff, "The statistical mechanical theory of solutions. I," J. Chem. Phys. **19**, 774–777 (1951).

[37] P. G. Kusalik and G. N. Patey, "The thermodynamic properties of electrolyte solutions: Some formal results," J. Chem. Phys. **86**, 5110–5116 (1987).

[38] M. Sevilla and R. Cortes-Huerto, "Connecting density fluctuations and Kirkwood–Buff integrals for finite-size systems," J. Chem. Phys. **156**, 044502 (2022).

[39] A. Jain, S. P. Ong, G. Hautier, W. Chen, W. D. Richards, S. Dacek, S. Cholia, D. Gunter, D. Skinner, G. Ceder, and K. A. Persson, "Commentary: The Materials Project: A materials genome approach to accelerating materials innovation," APL Mater. **1**, 011002 (2013).

[40] H. S. Harned, B. B. Owen, and C. V. King, "The physical chemistry of electrolytic solutions, third edition," J. Electrochem. Soc. **106**, 15C (1959).

[41] T. G. Pedersen, C. Dethlefsen, and A. Hvidt, "Volumetric properties of aqueous solutions of alkali halides," Carlsberg Res. Commun. **49**, 445–455 (1984).

[42] Z. Jing, Y. Zhou, T. Yamaguchi, K. Yoshida, K. Ikeda, K. Ohara, and G. Wang, "Hydration of alkali metal and halide ions from static and dynamic viewpoints," J. Phys. Chem. Lett. **14**, 6270–6277 (2023).

[43] B. M. Braun and H. Weingaertner, "Accurate self-diffusion coefficients of lithium(1+), sodium(1+), and cesium(1+) ions in aqueous alkali metal halide solutions from NMR spin-echo experiments," J. Phys. Chem. **92**, 1342–1346 (1988).

[44] S. Bouazizi and S. Nasr, "Local order in aqueous lithium chloride solutions as studied by X-ray scattering and molecular dynamics simulations," J. Mol. Struct. **837**, 206–213 (2007).

[45] R. M. Lawrence and R. F. Kruh, "X-ray diffraction studies of aqueous alkali-metal halide solutions," J. Chem. Phys. **47**, 4758–4765 (1967).

[46] T. Yamaguchi, H. Ohzono, M. Yamagami, K. Yoshida, and H. Wakita, "Ion hydration in aqueous solutions of lithium chloride, nickel chloride, and caesium chloride in ambient to supercritical water," J. Mol. Liq. **153**, 2–8 (2010).

[47] W. Wachter, S. Fernandez, R. Buchner, and G. Hefter, "Ion association and hydration in aqueous solutions of LiCl and Li$_2$SO$_4$ by dielectric spectroscopy," J. Phys. Chem. B **111**, 9010–9017 (2007).

[48] Z. Jin, X. Kong, Z. Wang, R. Zhang, L. Ma, and K. Lin, "Solvent shared ion pairs and direct contacted ion pairs in LiCl aqueous solution by IR ratio spectra," J. Solution Chem. **53**, 431–448 (2024).

[49] V. Mile, O. Gereben, S. Kohara, and L. Pusztai, "On the structure of aqueous cesium fluoride and cesium iodide solutions: Diffraction experiments, molecular dynamics simulations, and reverse Monte Carlo modeling," J. Phys. Chem. B **116**, 9758–9767 (2012).

[50] A. K. Soper and K. Weckström, "Ion solvation and water structure in potassium halide aqueous solutions," Biophys. Chem. **124**, 180–191 (2006).

[51] R. Buchner, W. Wachter, and G. Hefter, "Systematic variations of ion hydration in aqueous alkali metal fluoride solutions," J. Phys. Chem. B **123**, 10868–10876 (2019).

[52] I.-C. Yeh and G. Hummer, "System-size dependence of diffusion coefficients and viscosities from molecular dynamics simulations with periodic boundary conditions," J. Phys. Chem. B **108**, 15873–15879 (2004).

[53] M. J. Abraham, T. Murtola, R. Schulz, S. Páll, J. C. Smith, B. Hess, and E. Lindahl, "GROMACS: High performance molecular simulations through multi-level parallelism from laptops to supercomputers," SoftwareX **1–2**, 19 (2015).

[54] U. Essmann, L. Perera, M. L. Berkowitz, T. Darden, H. Lee, and L. G. Pedersen, "A smooth particle mesh Ewald method," J. Chem. Phys. **103**, 8577–8593 (1995).

[55] H. J. C. Berendsen, J. P. M. Postma, W. F. van Gunsteren, A. DiNola, and J. R. Haak, "Molecular dynamics with coupling to an external bath," J. Chem. Phys. **81**, 3684–3690 (1984).

[56] G. Bussi, D. Donadio, and M. Parrinello, "Canonical sampling through velocity rescaling," J. Chem. Phys. **126**, 014101 (2007).

[57] L. Bennett, B. Melchers, and B. Proppe, *Curta: A General-Purpose High-Performance Computer at ZEDAT* (Freie Universität Berlin, 2020).